Available online at www.sciencedirect.com
ScienceDirect
Polymer 48 (2007) 4777–4785
polymer
www.elsevier.com/locate/polymer

Multiple melting behavior of poly(3-hydroxybutyrate-*co*-3-hydroxyhexanoate) investigated by differential scanning calorimetry and infrared spectroscopy

Yun Hu [a], Jianming Zhang [a], Harumi Sato [a], Isao Noda [b], Yukihiro Ozaki [a,*]

[a] *Department of Chemistry, School of Science and Technology, Research Center for Environmental Friendly Polymers, Kwansei-Gakuin University, Sanda 669-1337, Japan*

[b] *The Procter & Gamble Company, 8611 Beckett Road, West Chester, OH 45069, USA*

Received 22 January 2007; received in revised form 26 May 2007; accepted 10 June 2007
Available online 15 June 2007

Abstract

The multiple melting behavior of poly(3-hydroxybutyrate-*co*-3-hydroxyhexanoate) (P(HB-*co*-HHx)) (HHx = 12 mol%) isothermally crystallized from the melt state has been characterized by differential scanning calorimetry (DSC) and Fourier transform infrared (FTIR) spectroscopy. The influence of different experimental variables (such as crystallization temperature, time, and heating rate) on the multiple melting behavior of P(HB-*co*-HHx) was investigated by using DSC. Moreover, it has been further examined by monitoring intensity changes of the characteristic IR bands during the subsequent heating process. For the isothermally crystallized P(HB-*co*-HHx) samples, triple melting peaks were observed upon heating. The weak lowest-temperature DSC endotherm I always appears at the position just above the crystallization temperature, and shifts to a higher temperature linearly with the logarithm of the crystallization time. The combination of DSC and IR results suggested that the occurrence of peak I was a result of the melting of crystals formed upon long-time annealing. As for the other two main melting endothermic peaks, endotherm II corresponds to the melting of crystals formed during the primary crystallization, and endotherm III is ascribed to the melting peak of the crystals formed by recrystallization during the heating process.

Keywords: Poly(3-hydroxybutyrate-*co*-3-hydroxyhexanoate); Infrared spectroscopy; Multiple melting behavior

1. Introduction

Multiple melting behavior (or double melting behavior) has been reported for many isothermally crystallized semicrystalline polymers, such as poly(ethylene terephthalate) (PET) [1–3], isotactic polystyrene (iPS) [4–7], poly(trimethylene terephthalate) (PTT) [8,9], poly(butylene succinate) (PBS) [10–12], poly(3-hydroxybutyrate) (PHB) and poly(3-hydroxybutyrate-*co*-3-hydroxyvalerate) (P(HB-*co*-HV)) [13–16]. It is an important subject of study in the field of polymer science to gain the basic understanding of the structural evolution during the heating process and to provide a new insight into the crystallization and melting process of semicrystalline polymer. A number of hypotheses were proposed to explain this phenomenon [1–19]. The most common mechanisms of multiple melting behavior include the dual morphology mechanism and the melting–recrystallization–remelting process. The former is based on the presence of two or more crystal modifications, different crystalline morphologies, or crystal lamellae of different stabilities. The latter is the case that crystallization produces primary crystals of lower degree of perfection or thinner lamellae, which can melt and recrystallize during the subsequent heat scan to yield crystals of higher perfection or greater thickness. Generally speaking, the origin of multiple melting behavior of polymers depends on their chemical structure and crystallization conditions.

* Corresponding author. Fax: +81 79 565 9077.
E-mail address: ozaki@kwansei.ac.jp (Y. Ozaki).

0032-3861/$ - see front matter © 2007 Published by Elsevier Ltd.
doi:10.1016/j.polymer.2007.06.016

Poly(3-hydroxybutyrate-*co*-3-hydroxyhexanoate) (P(HB-*co*-HHx)), a semicrystalline biodegradable polymer, exhibits a broad range of physical and mechanical properties depending on the comonomer content and the composition distribution. P(HB-*co*-HHx) copolymers with various HHx content can decrease crystallinity, reduce the crystallization rate, and increase flexibility compared to PHB homopolymer. Moreover, they have a wider thermal processing window, and a higher elongation-to-break value [20]. However, similar to PHB, it also exhibits a reduction in elongation-to-break and an increase in modulus over time [21]. To understand the physical and mechanical properties of P(HB-*co*-HHx), the solid structure, thermal behavior, and biodegradation mechanism of P(HB-*co*-HHx) have been studied extensively [20–32]. For instance, its crystallization and melting behavior has recently been investigated by wide-angle X-ray diffraction (WAXD) [24], infrared (IR) spectroscopy [25–29] and differential scanning calorimetry (DSC) [21–24,30–32], as it relates to many potential applications of this important class of polymers. In our previous study [24,27], the existence and thermally induced change of the C–H···O=C hydrogen bonding between the C=O group and the CH_3 group along the *a*-axis were explored in detail by combining WAXD and IR measurements for PHB and P(HB-*co*-HHx) copolymers.

Recently, Gunaratne et al. [14–16] carried out a series of experiments to investigate the melting behavior of PHB and P(HB-*co*-HV) with various HV content, which underwent various thermal histories, by using step-scan DSC, WAXD, and hot stage polarized optical microscopy (HSPOM). The experimental data revealed that the appearance of multiple melting peaks was due to the melting–recrystallization–remelting process occurring during heating. As for the multiple melting behavior of P(HB-*co*-HHx), not so many works have been reported [21–24,30–32]. A recent study conducted by Chen et al. [30] found that three melting endotherms were observed during the direct heating process after P(HB-*co*-HHx) (HHx = 15 mol%) was isothermally crystallized from the melt. On the basis of previous results from two-dimensional (2D) infrared correlation spectroscopy [25,28], they suggested that the broad melting shoulder ranging from 60 to 80 °C was ascribed to the premelting behavior of P(HB-*co*-HHx), which corresponds to an intermediate state between ordered crystalline and amorphous states. According to the study conducted by Gan et al. [31], it was proposed that the presence of HHx units results in the distribution of HB sequences with different length, which is responsible for the multiple melting behavior of P(HB-*co*-HHx). However, a reasonable model for interpreting these endothermic peaks has not been well established until now, especially the presence of a minor endothermic peak that appears just above the crystallization temperature. Thus, further investigation is necessary to gain a deeper understanding of the subsequent multiple melting behavior observed in isothermally melt-crystallized P(HB-*co*-HHx).

Fourier transform infrared (FTIR) spectroscopy is a powerful technique, and sensitive to molecular interactions and structural conformational changes of polymer. It allows one to gain insight into the structural changes of semicrystalline polymers during the crystallization and melting process by monitoring changes of the characteristic bands, which are correlated with the crystalline, amorphous states and conformations [7,25–29,36–39]. The present study focuses on the investigation of multiple melting behavior of P(HB-*co*-HHx) after experiencing the isothermal melt-crystallization. Accordingly, the possible explanation for the complex multiple melting behavior on the subsequent heating process will be discussed by combining DSC and FTIR analysis.

2. Experimental

2.1. Materials

Bacterially synthesized P(HB-*co*-HHx) (HHx = 12 mol%) was obtained from the Procter & Gamble Company, Cincinnati, OH. P(HB-*co*-HHx) was purified first by dissolving it in hot chloroform, and then precipitating in methanol, and vacuum-drying at 60 °C for 24 h. Chloroform and methanol were purchased from Wako Pure Chemical Industries, Ltd, Osaka, Japan.

2.2. DSC measurement

Thermal analysis was carried out with a Perkin Elmer Pyris 6 apparatus, under a nitrogen purge. High purity indium and zinc were used for temperature calibration and indium standard was used for calibration of the heat of fusion (ΔH). To avoid an uneven thermal conduction of the samples, which may cause different amounts of broadening and shifting of the peak positions, the aluminum pans were always filled with the same quantity of specimen, about 5(±0.2) mg. P(HB-*co*-HHx) samples were heated to a fixed temperature at 155 °C for 3 min to remove any nuclei in them by using a Mettler FP82HT hot stage. Then, the melted samples were rapidly transferred to a predetermined crystallization temperature (T_c). Isothermal crystallization was carried out at various temperatures ranging from 60 to 95 °C, where the sample was held until the crystallization process was considered complete (when no significant change in the heat flow as a function of time was further observed). Freshly prepared samples were used for each case to minimize the cumulative effect of thermal degradation of sample. Unless, otherwise specified, DSC melting curves were obtained at 10 °C min^{-1} after rapid cooling of a sample from T_c to 30 °C and holding it at 30 °C for 2 min.

2.3. IR measurement

For the IR measurement, P(HB-*co*-HHx) films were cast on KBr windows from 1% (w/v) chloroform solution. After the majority of the solvent had evaporated, the films were placed under vacuum at room temperature for 48 h to remove the residual solvent. The KBr windows with the sample were set on a homemade variable temperature cell, which was placed in the sample compartment of a Thermo Nicolet Magna 870 spectrometer equipped with a MCT detector. The spectra of samples were measured at 2 cm^{-1} spectral resolution with 16 scans

coadded. To prepare samples melt-crystallized at different temperatures, the same procedures in the DSC are used. For the melting process study, the heating rate of 2 °C min^{-1} was used.

2.4. WAXD measurement

To investigate the crystalline structure of P(HB-*co*-HHx) sample, wide-angle X-ray diffraction measurements were carried out on Rigaku RINT2100 system by using Cu Kα radiation ($\lambda = 0.15418$ nm, 50 kV, 40 mA) in the scattering angle range of $2\theta = 11-19°$ at a scan speed of 1°/min. The temperature was increased at a rate of ca. 2 °C min^{-1} and WAXD data recorded at every 10 °C ranging from 70 to 130 °C. Before each WAXD measurement, the cell was maintained at that temperature for 5 min to make the sample equilibrated.

3. Results and discussion

The main difference in chemical structures between PHB and P(HB-*co*-HHx) lies in the length of the alkyl side chain attached to the polymer backbone, as depicted in Fig. 1. By introducing the bulky propyl side group onto the main chain, long-range packing becomes disrupted. Thus, the crystallization and melting behavior of P(HB-*co*-HHx) shows some differences from those of PHB. For instance, the crystallinity decreases, rate of crystallization reduces, and the multiple melting peaks become evident. To shed more light onto the origin of multiple melting behavior of P(HB-*co*-HHx), DSC and IR measurements have been carried out.

3.1. Multiple melting behavior of isothermally crystallized P(HB-co-HHx) investigated by DSC

The effect of crystallization temperature (T_c) on the subsequent melting behavior of P(HB-*co*-HHx) at a constant heating rate of 10 °C min^{-1} is illustrated in Fig. 2. The total crystallization time required for the completion of crystallization at investigated T_c is varied and found to be an increasing function of T_c.

According to Fig. 2, the subsequent melting DSC curves of P(HB-*co*-HHx) show a broader melting range compared with those of homopolymer PHB. Three endothermic peaks, labeled as I, II, and III, in the order of increasing temperature are observed in the melting curves. Accordingly, temperatures for these endotherms are denoted as the low-melting peak temperature T_I, the middle-melting peak temperature T_{II}, and the high-melting temperature T_{III}. All these endothermic peaks shift to higher temperatures with increase in T_c. In comparison, the

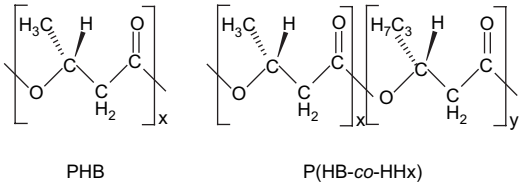

Fig. 1. Chemical structures of PHB and P(HB-*co*-HHx).

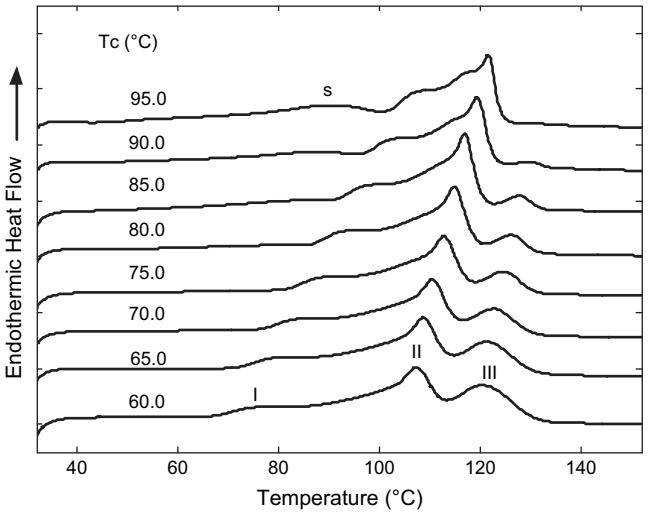

Fig. 2. Subsequent melting curves for P(HB-*co*-HHx) samples isothermally crystallized from the melt state at different crystallization temperatures. Peaks I, II, and III denote the low-, middle- and high-temperature melting endotherms, respectively.

melting curves for isothermally melt-crystallized PHB homopolymer typically show only a single melting peak or occasionary double peaks. The appearance of such double peaks of PHB depends on the heating rate or crystallization conditions, and they are mainly caused by the melt–recrystallization–remelting mechanism during the heating process [13–16]. However, the endothermic peak I is rarely observed in isothermally crystallized PHB samples [13–16,31]. It is known that the crystallization of P(HB-*co*-HHx) is hindered, and imperfect crystals are formed with increasing HHx content due to shorter HB sequence lengths. It is interesting to note that when T_c is above 85 °C, a broad small endothermic peak labeled S can also be detected below T_c. To clarify the origin of this peak, the melting curve of a sample directly heated from the crystallization temperature (i.e., instead of cooling first to 30 °C) was measured. In this measurement this sub-T_c peak could not be detected. The experimental result suggested that this additional peak might be associated with the melting of material which was crystallized during the cooling from the annealing temperature to 30 °C and maintaining it for 2 min [22,31,40]. Quantitative information for all of the subsequent melting thermograms recorded is displayed in Fig. 3, and the dotted lines show the results of linear fitting curves.

The low-melting temperature of minor endotherm I shifts to higher temperature with increasing T_c but appears at ca. 10–15 °C above the melt-crystallization or annealing temperature, and is almost parallel to the line $T_m = T_c$. This result is a typical characteristics of the so-called annealing peak [3,4,7,31]. Similarly, the endotherms II and III steadily increase with increasing T_c, but there is an increase in the area under the endothermic II peak, and decrease of the area under the endothermic III peak. This observation suggests that at higher T_c, the crystallization proceeds at a slower rate, accompanied by simultaneous annealing, resulting in the formation of more perfect crystals. Thus, the fraction that would undergo recrystallization on heating decreases.

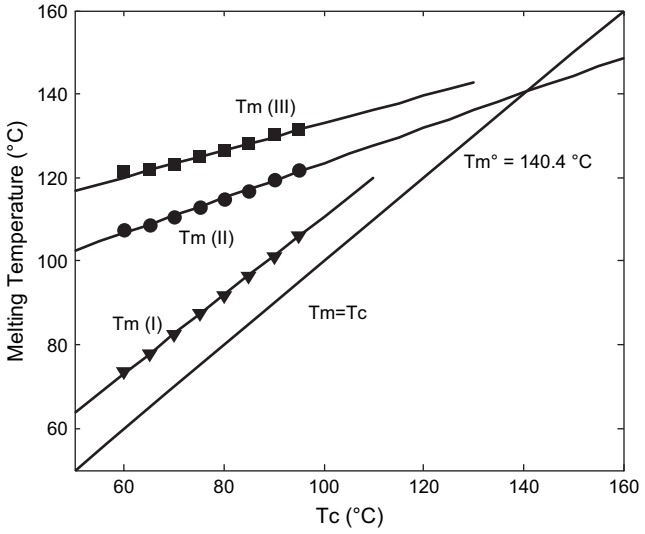

Fig. 3. Melting temperatures versus crystallization temperature for P(HB-*co*-HHx) isothermally melt-crystallized at different temperatures.

Fig. 4 shows the temperature dependence of the WAXD profiles of the P(HB-*co*-HHx) sample isothermally melt-crystallized at 70 °C for 6 h. The profile measured at 70 °C clearly shows the crystalline reflections of (020) and (110) plane, which are the major reflections of PHB crystal. This result indicated that HHx units cannot crystallize in the sequences of HB units and act as defects in the PHB crystal lattice during the melt-crystallization process. As can be seen from the figure, the positions of diffraction peaks from the crystalline state remain invariant up to 120 °C, but the crystallinity is reduced with increasing temperature. When the temperature is raised to 130 °C, no sign of crystallinity was observed. The significant decrease in crystallinity starts from 110 °C, reflecting the melting of primary crystals, which is consistent with those from DSC. Therefore, the effect of various crystal modifications on the multiple melting behavior can be precluded.

To explore the specific sequence of crystal formation during the crystallization process, samples from the melt were also crystallized at a certain crystallization temperature for various period of time (t_c) and then heated directly from the crystallization temperature without cooling. Fig. 5 displays the melting endotherms of P(HB-*co*-HHx) crystallized at 70 °C for various periods of time. As the time for crystallization increased from 5 to 60 min, the melting enthalpy became larger, showing the growth of crystals. When $t_c = 10$ min, endotherms II and III appear about 110 and 123 °C simultaneously. Of note is that the minor endotherm I has not been observed in subsequent melting endotherms recorded at early stages of crystallization (i.e., partial crystallization for short time intervals at given T_c) until $t_c = 40$ min. As the crystallization period becomes longer, endotherm I becomes more apparent and moves to a higher temperature, while endotherms II and III do not show such obvious change after $t_c = 60$ min. The same observation was obtained for the sample crystallized at 60 °C.

To further investigate the nature of this minor endotherm I, a partial melting experiment was performed. Firstly, the sample was crystallized at 60 °C for 60 min, and heated to 90 °C at 5 °C min^{-1}. Then, it was kept constant for 10 min to undergo the partial melting followed by rapid cooling to 30 °C and then heated again. Fig. 6 shows the corresponding results, where the three endothermic peaks still occur for this partially melted sample (curve a). It is interesting to note that the endothermic peaks II and III for the partially melted sample are identical to

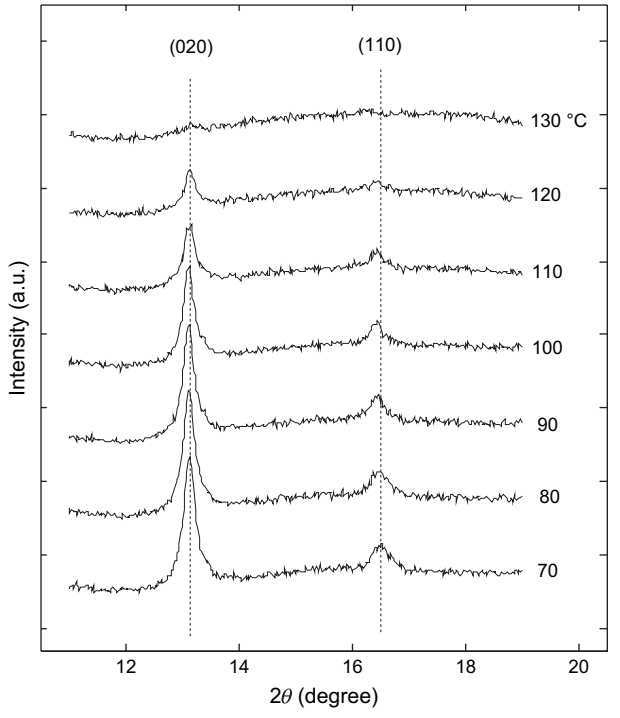

Fig. 4. Temperature dependence of the X-ray diffraction of the P(HB-*co*-HHx) sample isothermally melt-crystallized at 70 °C for 6 h over a temperature range from 70 to 130 °C.

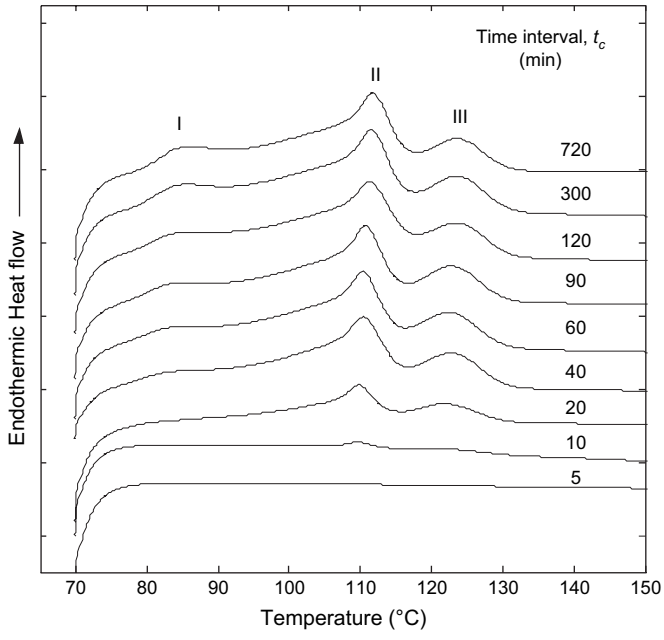

Fig. 5. Subsequent melting curves for P(HB-*co*-HHx) (HHx = 12 mol%) samples after partial crystallization at 70 °C for different time intervals as indicated.

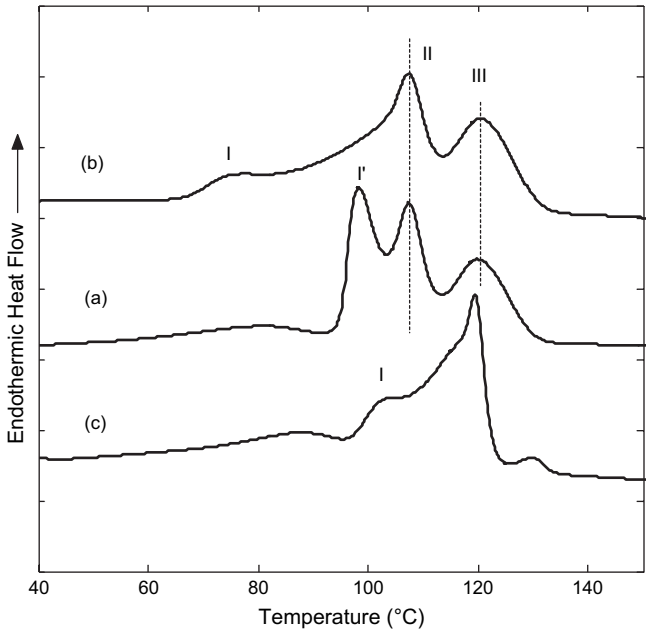

Fig. 6. A DSC curve for a sample partially melted at $T_{pm} = 90\ ^{\circ}C$ for 10 min after isothermal crystallization at $T_c = 60\ ^{\circ}C$ for 60 min (a). DSC curves for samples isothermally crystallized at (b) 60 °C and (c) 90 °C are also shown for comparison.

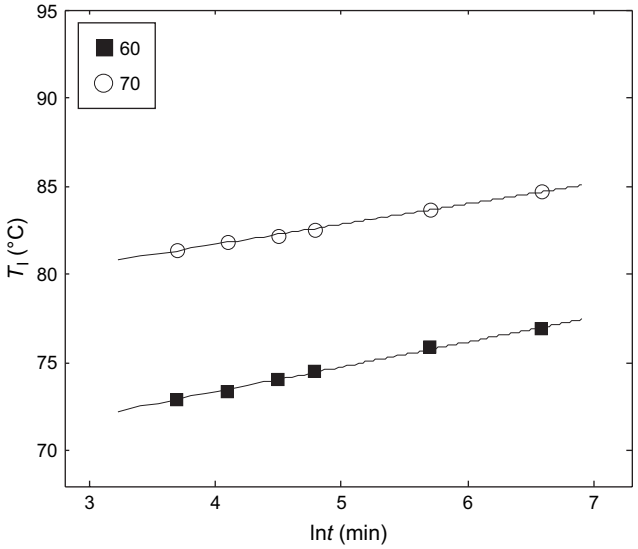

Fig. 7. The dependence of T_I on crystallization temperature and time.

those for the sample crystallized at 60 °C (curve b), while the new endotherm I′ is close to that for the sample crystallized at 90 °C (curve c). During the partial melting at $T_{pm} = 90\ ^{\circ}C$, crystals responsible for the minor endotherm I melt, and they reorganize into more stable crystals, which cause the new endoderm I′ observed from the partial melting experiment. This result clearly implies that the development of a crystalline structure that corresponds to the low-melting peak I′ occurs during annealing at 90 °C. Concerning the middle- and high-temperature peaks (II and III), they remain unchanged during the partial melting process. Thus it is suggested that the peak II is related to the melting of primary crystals formed during the initial crystallization at 60 °C, and the peak III is associated with the melting of primary crystals recrystallized during the heating scan. The same results were obtained from the partial melting experiment of sample crystallized at 70 °C. The present result is somewhat different from the previously reported one [31], which showed that melting peak I disappears and peak III becomes hardly detectable after the annealing treatment. Accordingly, it was indicated in Ref. [31] that crystals with peak III may have a close relationship with those with peak I, which have poor crystal structures. However, the present study shows the melting behavior of crystals I does not seem to have such relationship with that of crystals III.

Fig. 7 shows that the T_I values increase linearly with the logarithm of the crystallization time at given T_c. Such logarithmic time dependence is conventionally associated with the secondary crystallization [1,3,19]. Furthermore, the magnitude of this peak area increases with time. Application of Flory's equilibrium model [33–35] to the P(HB-*co*-HHx) random copolymer, it is suggested that the endotherm I is caused by the melting of crystals composed of HB sequences with length shorter than the critical length, and it may arise from small size crystalline domains located between or outside the regular crystals. Accordingly, the endotherm II may be related to the melting of regular crystals composed of HB sequences with length longer than the critical length formed at given T_c. Therefore, the coexistence of two types of crystals in P(HB-*co*-HHx) has been suggested. Considering that the high HHx units produce a number of amorphous parts, together with the above observations, this weak DSC endotherm I is possibly caused by the melting of imperfect crystallites formed upon long-time annealing.

It is well known that the heating rate dependence on the multiple melting behavior is often cited as evidence in favor of the "melting-recrystallization" model [4]. Fig. 8 shows the heating dependence of the melting behavior for P(HB-*co*-HHx) crystallized at 70 °C for 60 min. It is apparent that for the sample crystallized at 70 °C, the endotherms I and II shift toward higher temperature, while the endotherm III shifts to the opposite direction accompanied with the decrease in magnitude with increasing heating rate. When the heating rate is equal to $30\ ^{\circ}C\ min^{-1}$, peak III merges into peak II. This result suggests that, during a heating scan, the less stable fraction of the primary crystallites melts and recrystallizes and, upon further heating, the recrystallized crystallites melt again, giving rise to the formation of peak III. The higher the heating rate used, the shorter the time being available for the diffusion of the molecular segment to the growing crystallites. Thus, it is reasonable to conclude that the peak II should be attributed to the melting of crystals formed at T_c, and the peak III may be due to the melting of crystals formed by the partial melting and recrysllization process [30–32].

As mentioned above, endotherm II corresponds to the melting of the primary crystals formed at a certain crystallization temperature. It is possible to estimate approximately the equilibrium melting point of this P(HB-*co*-HHx) sample having the HHx content of 12 mol% to be 140.4 °C by the

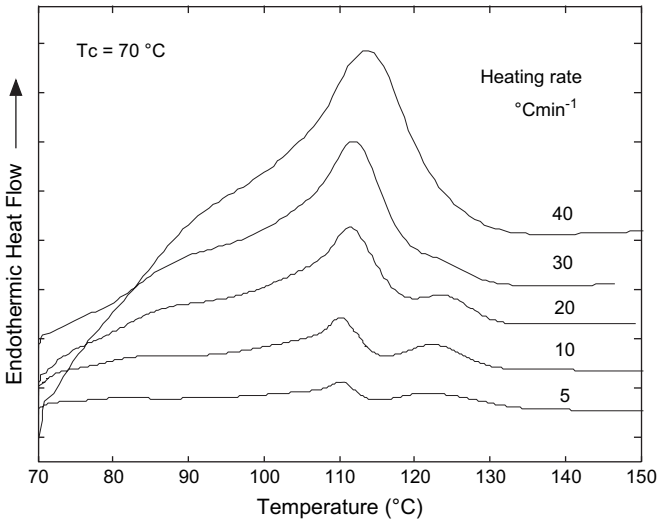

Fig. 8. Subsequent melting curves for P(HB-*co*-HHx) samples using different heating rates ranging from 5 to 40 °C min^{-1} after isothermal crystallization at 70 °C for 60 min.

Hoffman–Weeks extrapolation [41], which is substantially lower than that of PHB homopolymer [42].

3.2. In situ FTIR study on the melting process of isothermally crystallized P(HB-co-HHx)

In addition to DSC, FTIR is also a powerful technique to investigate the crystallization and melting behavior of semicrystalline polymer. It allows one to in situ monitor changes of characteristic bands, which are sensitive to structural conformations and molecular environments of polymer, and the presence of structural changes on a molecular level [7,25–29,36–39]. Fig. 9 shows temperature-dependent IR spectra in the range of 3020–2830, 1780–1670, and 1500–800 cm^{-1} recorded over a temperature range from 70 to 150 °C at a 4 °C temperature interval after P(HB-*co*-HHx) sample is annealed at 70 °C for 6 h. The bands in these three regions are, respectively, due to the C–H stretching vibration, C=O stretching vibration, and the CH_3, CH_2, CH bending vibration, the C–O–C and C–C stretching vibration. It can be seen that many bands show peak intensity changes and shifts during the heating process, unambiguously indicating that some changes happen in the crystal structure of P(HB-*co*-HHx). The overall spectral variations induced by the heating are similar to those of PHB, whereas the crystallinity and the melting temperature are lower compared with those of PHB. The corresponding second derivatives of the spectra measured at the beginning (in the semicrystalline state) and the end (in the amorphous state) are also presented in the top panel of Fig. 9. Noted that a band at 2962 cm^{-1} in the corresponding second derivative of the amorphous spectrum of P(HB-*co*-HHx) in Fig. 9a is detected. A similar band could not be found in the amorphous spectrum of PHB, indicating that this band is caused by the incorporation of bulky propyl side chain, which is attributed to the asymmetric stretching mode of the CH_3 group in the branched alkyl group [27,28]. The temperature-induced intensity changes of this band is

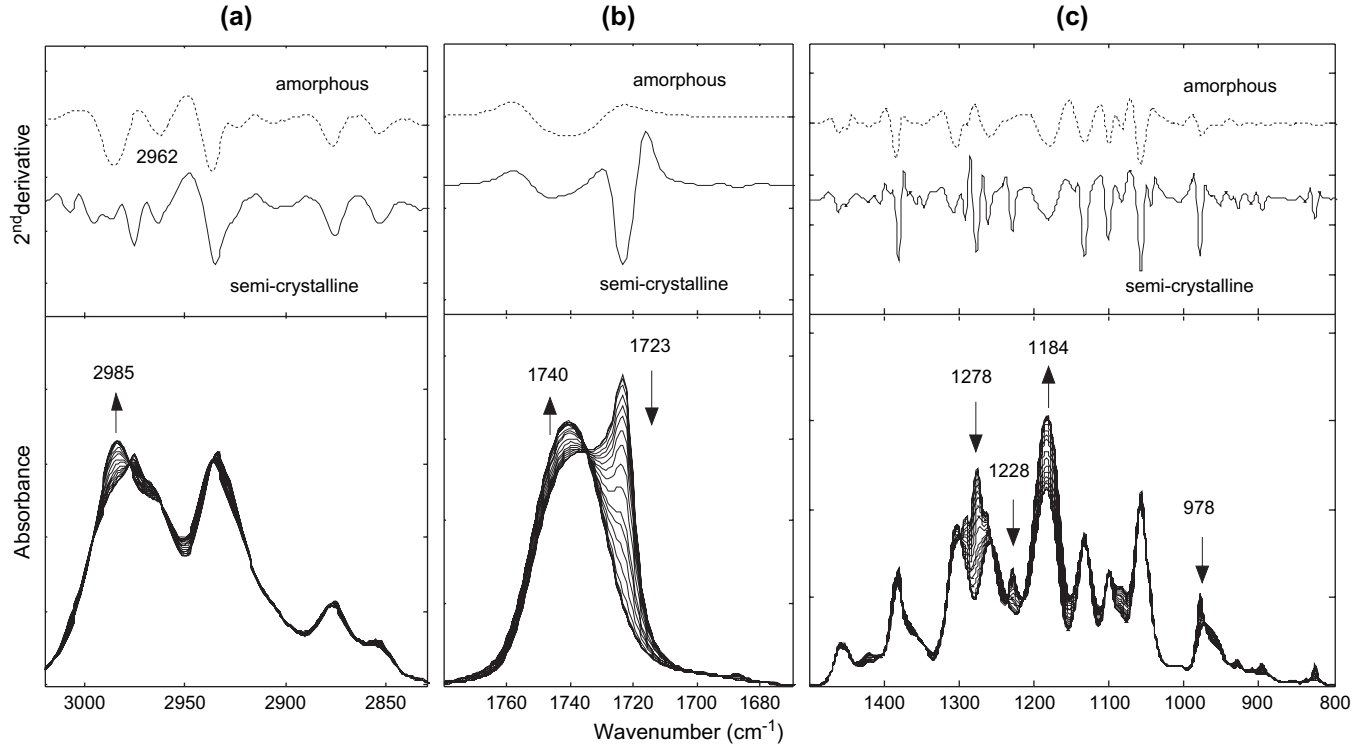

Fig. 9. Temperature-dependent IR spectra and their second derivatives collected in the range of (a) 3020–2830 cm^{-1}; (b) 1780–1670 cm^{-1}; (c) 1500–800 cm^{-1} during the heating process after P(HB-*co*-HHx) isothermally melt-crystallized at 70 °C for 6 h. Bands indicated by "↓" and "↑" correspond to the crystalline and amorphous ones, respectively.

not obvious, which provides an evidence to confirm that HHx units act as non-crystallizable component. It was well documented that the intensity of the band located at 1184 cm^{-1} increases with temperature, which is assigned to the asymmetric stretching vibration of the C–O–C group. Accordingly, it is attributed to the amorphous band. The band at 1228 cm^{-1} is due to the CH_2 wagging and twisting modes and ascribed to the conformational band of the helical chains, since no amorphous band of the same group could be found [26]. The bands at 1740 and 1723 cm^{-1} are, respectively, ascribed to the C=O stretching vibrations of the amorphous and crystalline carbonyl group [25–29].

The in situ monitoring of the intensity changes in characteristic IR bands with temperature should help explaining the origins of multiple melting behavior of P(HB-*co*-HHx). Fig. 10 shows the plots of the normalized intensity changes of the bands at 1723, 1184, and 1228 cm^{-1} as a function of temperature, which are obtained from the heating scan of the P(HB-*co*-HHx) sample crystallized at 70 °C for 6 h. It is apparent that the intensity changes of these bands are related to the crystalline structure changes during the heating process. In Fig. 10a, it is clearly found that there are two stepwise intensity reduction of the 1723 cm^{-1} band at 80 and 106 °C. Around these two temperatures, the intensity of the crystalline band at 1723 cm^{-1} (Fig. 10a) decreases more quickly accompanied by the intensity increase of amorphous band at 1184 cm^{-1} (Fig. 10b). Likewise, the conformational band of the helical chains at 1228 cm^{-1} (Fig. 10c) shows a similar trend with increment of temperature. Because the intensity changes of crystalline, amorphous, and helical conformation bands can be directly related to the change of crystallinity, the above observation suggests that some amount of crystals have melted at these temperatures [7].

To further clarify the subtle shift in the trends of intensity changes, the decaying rate [38,39], defined as dH/dT (dH and dT are, respectively, the small changes of the normalized intensity and the temperature with heating) is calculated to describe the melting behavior, shown in the corresponding inserted figure. The plot of the decaying rate is comparable with the corresponding DSC melting curve, and can be used here to monitor not only the crystallinity but also the structural evolution of crystals during the heating process. It now

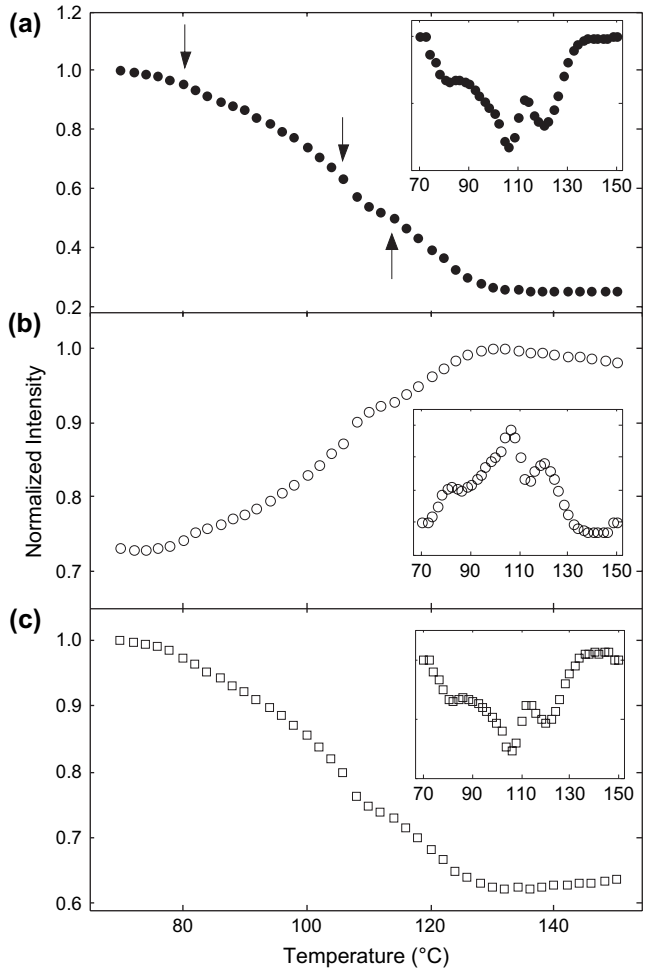

Fig. 10. Normalized intensity changes in the bands at (a) 1723 (●), (b) 1184 (○), and (c) 1228 (□) cm^{-1} as a function of temperature during the heating process for P(HB-*co*-HHx). The sample was melt-crystallized at 70 °C for 6 h. The inserted graphs show the decaying rates of these bands with temperature.

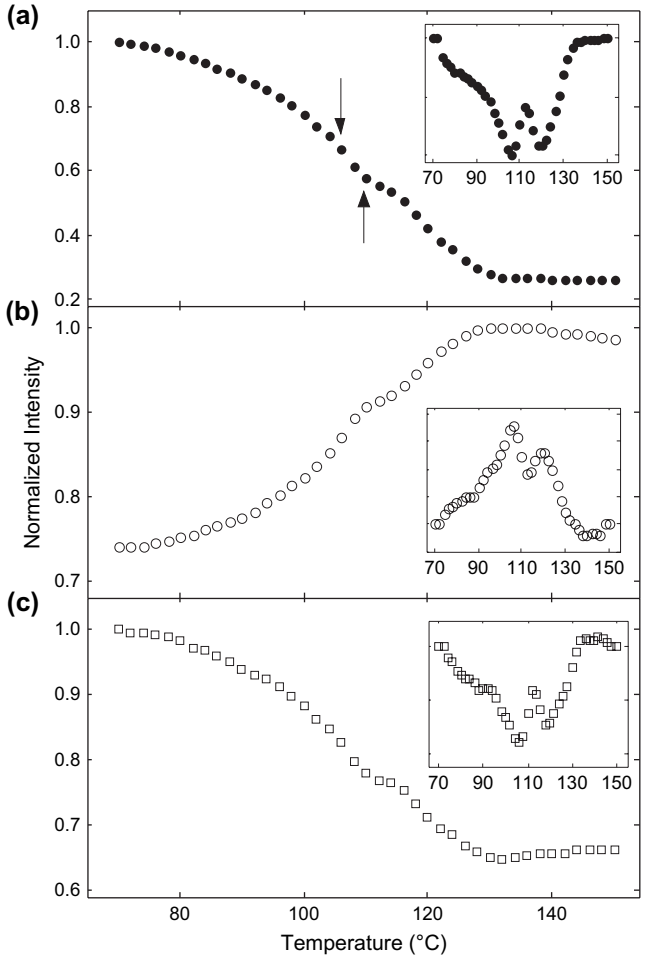

Fig. 11. Normalized intensity changes in the bands at (a) 1723 (●), (b) 1184 (○), and (c) 1228 (□) cm^{-1} as a function of temperature during the heating process for P(HB-*co*-HHx). The sample was melt-crystallized at 70 °C for 40 min. The inserted graphs show the decaying rates of these bands with temperature.

becomes obvious that the peak intensity changes of these bands decrease or increase continuously with three distinct transitions, which can correspond to the three melting peaks in the DSC curves.

To further investigate the intensity transition around 82 °C, the normalized intensity changes of these characteristic bands of the sample crystallized at 70 °C for only 40 min are plotted in Fig. 11 as a function of temperature. Particular attention should be paid to the inserted figure. The decaying rates of these bands with temperature show no distinct intensity transition around at 82 °C, implying that little crystals melted at this temperature. Combining with previous DSC results, it is reasonable to suggest that the intensity change for this peak is caused by the melting of some crystals formed during the long-time annealing. Moreover, these crystals have the same crystal structure as the primary crystals formed at T_c judging from the IR spectral variations. However, they may have low degree of perfection and melted at a lower melting temperature. Thus, this result provides further evidence to support the assertion that the multiple melting behavior is not caused by multiple crystalline polymorphs.

As can be seen from Figs. 10 and 11, the last two transitions (two melting peaks) appear in both samples crystallized for 40 min and 6 h. Between them, no evident intensity increase for the crystalline band and intensity decrease for the amorphous band could be identified directly from 108 to 114 °C. However, it is found that there is an inflection point, as well as the appearance of two peaks in the plots of decaying rates of these bands, indicating the intensity changes of these bands are not monotonically decreasing or increasing. This result provides the evidence to support the occurrence of the partial melting and recrystallization process in this temperature range. It may be explained that the melting of primary crystals at T_c is followed by instantaneous recrystallization, i.e., the recrystallization rate of these molten crystals may be too fast to be resolved clearly. Hence, the obvious intensity decrease of amorphous band and intensity increase of crystalline band during the recrystallization process cannot be detected. In the case of PHB, it can form relatively perfect crystals during the isothermal crystallization process, which is difficult to be recrystallized. Thus, the intensity change of these bands in the melting temperature range usually shows one transition. This result is in agreement with that obtained from DSC experiments.

4. Conclusions

The multiple melting behavior of the isothermally melt-crystallized copolymer P(HB-*co*-HHx) was studied by combining DSC and FTIR analysis. Three endothermic peaks were observed during the subsequent heating scan. By monitoring the intensity changes of the crystalline, amorphous, and conformation sensitive bands in the temperature-induced FTIR spectra, the origin of the multiple melting temperatures phenomenon is discussed. It is suggested that the crystals represented by the endothermic peak I, having the lowest melting temperature, are formed during long-time annealing. The other two main melting edothermic peaks II and III are caused by the model of melting, recrystallization and remelting of PHB crystals during the heating process.

Acknowledgements

This work was partially supported by ‘‘Open Research Center’’ project for private universities: matching fund subsidy from MEXT (Ministry of Education, Culture, Sports, Science and Technology), 2001–2008. This work was also supported by Kwansei-Gakuin University ‘‘Special Research’’ project, 2004–2008.

References

[1] Kong Y, Hay JN. Polymer 2003;44:623–33.
[2] Minakov AA, Mordvintsev DA, Schick C. Polymer 2004;45:3755–63.
[3] Bonnet M, Rogausch KD, Petermann J. Colloid Polym Sci 1999; 277:513–8.
[4] Liu T, Petermann J. Polymer 2001;42:6453–61.
[5] Liu T, Yan S, Bonnet M, Lieberwirth I, Rogausch KD, Petermann J. J Mater Sci 2000;35:5047–55.
[6] Liu T, Petermann J, He C, Liu Z, Chung TS. Macromolecules 2001; 34:4305–7.
[7] Duan YX, Zhang JM, Shen DY, Yan SK. Macromolecules 2003; 36:4874–9.
[8] Chung WT, Yeh WJ, Hong PD. J Appl Polym Sci 2002;83:2426–33.
[9] Srimoaon P, Dangseeyun N, Supaphol P. Eur Polym J 2004;40:599–608.
[10] Yoo ES, Im SS. J Polym Sci Part B Polym Phys 1999;37:1357–66.
[11] Yasuniwa M, Satou T. J Polym Sci Part B Polym Phys 2002;40:2411–20.
[12] Yasuniwa M, Tsubakihara S, Satou T, Iura K. J Polym Sci Part B Polym Phys 2005;43:2039–47.
[13] Owen AJ, Heinzel J, Škrbić Ž, Divjaković V. Polymer 1992;33:1563–7.
[14] Gunaratne LMWK, Shanks RA, Amarasinghe G. Thermochim Acta 2004; 423:127–35.
[15] Gunaratne LMWK, Shanks RA. Thermochim Acta 2005;430:183–90.
[16] Gunaratne LMWK, Shanks RA. Eur Polym J 2005;41:2980–8.
[17] Papageorgiou GZ, Achilias DS, Karayannidis GP, Bikiaris DN, Roupakias C, Litsardakis G. Eur Polym J 2006;42:434–45.
[18] Sun YS, Woo EM. Macromolecules 1999;32:7836–44.
[19] Wang YM, Bhattacharya M, Mano JF. J Polym Sci Part B Polym Phys 2005;43:3077–82.
[20] Doi Y, Kitamura S, Abe H. Macromolecules 1995;28:4822–8.
[21] Asrar J, Valentin HE, Berger PA, Tran M, Padgette SR, Garbow JR. Biomacromolecules 2002;3:1006–12.
[22] Abe H, Doi Y, Aoki H, Akehata T. Macromolecules 1998;31:1791–7.
[23] Feng L, Watanabe T, Wang Y, Kichise T, Fukuchi T, Chen GQ, et al. Biomacromolecules 2002;3:1071–7.
[24] Sato H, Nakamura M, Padermshoke A, Yamaguchi H, Terauchi H, Ekgasit S, et al. Macromolecules 2004;37:3763–9.
[25] Wu Q, Tian G, Sun SQ, Noda I, Chen GQ. J Appl Polym Sci 2001; 82:934–40.
[26] Xu J, Guo BH, Yang R, Wu Q, Chen GQ, Zhang ZM. Polymer 2002;43:6893–9.
[27] Sato H, Murakami R, Padermshoke A, Hirose F, Senda K, Noda I, et al. Macromolecules 2004;37:7203–13.
[28] Padermshoke A, Sato H, Katsumoto Y, Ekgasit S, Noda I, Ozaki Y. Vib Spectrosc 2004;36:241–9.
[29] Sato H, Padermshoke A, Nakamura M, Murakami R, Hirose F, Senda K, et al. Macromol Symposia 2005;220:123–38.
[30] Chen C, Cheung MK, Yu PHF. Polym Int 2005;54:1055–64.
[31] Gan ZH, Kuwabara K, Abe H, Doi Y. Biodegradable polymers and plastics. In: Proceedings of the seventh world conference on biodegradable polymers & plastics. Terrenia, Italy; June 4–8, 2002 (2003), Meeting Date 2002. p. 167–84.

[32] Watanabe T, He Y, Fukuchi T, Inoue Y. Macromol Biosci 2001;1:75–83.
[33] Flory PJ. J Chem Phys 1949;12:223–40.
[34] Flory PJ. Trans Faraday Soc 1955;51:848–57.
[35] Alizadeh A, Richardson L, Xu J, McCartney S, Marand H. Macromolecules 1999;32:6221–35.
[36] Wang S, Shen DY, Qian RY. J Appl Polym Sci 1996;60:1385–9.
[37] Zhu XY, Yan DY. Macromol Chem Phys 2001;202:1109–13.
[38] Zhu B, He Y, Asakawa N, Yoshie N, Nishida H, Inoue Y. Macromolecules 2005;38:6455–65.
[39] Zhu B, He Y, Asakawa N, Nishida H, Inoue Y. Macromolecules 2006;39:194–203.
[40] Abe H, Kikkawa Y, Aoki H, Akehata T, Iwata T, Doi Y. Int J Biol Macromol 1999;25:177–83.
[41] Hoffman JD, Weeks JJ. J Res Natl Bur Stand 1962;A66:13–28.
[42] Organ SJ, Barham PJ. Polymer 1993;34:2169–74.